Molecular Crystals and Liquid Crystals
Publication details, including instructions for authors and subscription information:
http://www.tandfonline.com/loi/gmcl20

Synthesis and Characterization of Supramolecular Hydrogen-Bonded Liquid Crystals Comprising of p-n-Alkyloxy Benzoic Acids with Suberic Acid and Pimelic Acid

P. Subhapriya [a], P. S. Vijayanand [a] & M. L. N. Madhu Mohan [b]
[a] Department of Physical Sciences, Bannari Amman Institute of Technology, Sathyamangalam, India
[b] Liquid Crystal Research Laboratory (LCRL), Bannari Amman Institute of Technology, Sathyamangalam, India
Version of record first published: 18 Jan 2013.

To cite this article: P. Subhapriya , P. S. Vijayanand & M. L. N. Madhu Mohan (2013): Synthesis and Characterization of Supramolecular Hydrogen-Bonded Liquid Crystals Comprising of p-n-Alkyloxy Benzoic Acids with Suberic Acid and Pimelic Acid, Molecular Crystals and Liquid Crystals, 571:1, 40-56

To link to this article: http://dx.doi.org/10.1080/15421406.2012.741338

Mol. Cryst. Liq. Cryst., Vol. 571: pp. 40–56, 2013

ISSN: 1542-1406 print/1563-5287 online
DOI: 10.1080/15421406.2012.741338

Synthesis and Characterization of Supramolecular Hydrogen-Bonded Liquid Crystals Comprising of p-n-Alkyloxy Benzoic Acids with Suberic Acid and Pimelic Acid

P. SUBHAPRIYA,[1] P. S. VIJAYANAND,[1]
AND M. L. N. MADHU MOHAN[2,*]

[1]Department of Physical Sciences, Bannari Amman Institute of Technology, Sathyamangalam, India
[2]Liquid Crystal Research Laboratory (LCRL), Bannari Amman Institute of Technology, Sathyamangalam, India

Two series of supramolecular hydrogen-bonded liquid crystalline complexes have been designed and synthesized. A successful attempt has been made to form hydrogen bond between Suberic acid (SA) and Pimelic acid (PA) with p-n-alkyloxy benzoic acids (nBAO) by varying the respective alkyloxy carbon number. The first homologous series comprises of Suberic acid and p-n-alkyloxy benzoic acids (SA+nBAO), while the another series is formed between Pimelic acid and p-n-alkyloxy benzoic acids (PA+nBAO), where n represents the alkyloxy carbon number which varies from 5 to 12. These two homologous series are analyzed by polarizing optical microscope, differential scanning calorimetry, Fourier transform infrared spectroscopy (FTIR), and proton NMR studies. The formation of intermolecular hydrogen bond is evinced through FTIR and ^{1}H-NMR. An interesting feature of PA+nBAO homologues series is the inducement of tilted smectic C phase with increasing carbon chain length. In the SA+nBAO homologues series odd–even effect is observed at isotropic to nematic transition temperatures. Phase diagrams of the above complexes are constructed and compared.

Keywords ^{1}H-NMR; FT-IR; intermolecular hydrogen bonding; odd–even effect; phase diagram; smectic C phase

1. Introduction

Hydrogen bonding is one of the key interactions for chemical and biological process in nature. For molecular aggregation, hydrogen bonding plays an important role in the association of molecules. In liquid crystals (LCs), mesomorphism results from the proper combination of molecular interactions and the shape of molecules. Dipole–dipole interaction has long been taken into consideration in the design of liquid-crystalline molecules. In contrast and with few exceptions, intermolecular hydrogen bonds, that are stronger than dipole–dipole interaction had been considered to be deleterious for thermotropic liquid

*Address correspondence to M. L. N. Madhu Mohan, Department of Physical Science, Bannari Amman Institute of Technology Sathyamangalam 638 401, India. Tel.: +91 9442437480; Fax: +91 4295 223 775. E-mail: mln.madhu@gmail.com

crystallinity in the past because in many cases they cause molecular association that raise melting temperature or destroy molecular order of the mesophase. Moreover hydrogen bond (H-bond) will behave as a strong intermolecular noncovalent force, and plays an important role in biological systems but also serves as a specific molecular interaction for crystal packing [1–5].

Supramolecular assemblies built up from hydrogen-bonding interactions have received much attention due to their attractive properties such as photochromism, optical activity and electrosensitivity, etc. [6,7]. Understanding the noncovalent interactions role is a major challenge for the rational design of well-defined supramolecular structures and materials. Therefore, recently the principles governing noncovalent self-assembly, especially hydrogen bonding have been studied intensively [8,9]. The well-defined self-assembly architectures may be induced by the selective association of molecular components through non covalent interactions and have attracted much attention because these materials are good candidates for the next generation of materials [10]. Over the past few decades, scientists have developed new approaches to obtain a wide variety of LC molecules. These materials have more potential applications in various fields such as display material, information charge, transportation, transformation, and molecular sensing by further functionalization. The use of specific interactions namely hydrogen bonding is one of the versatile approach [11]. Thus, the hydrogen bond acts as a linkage to hold the two rigid components together and forms mesogenic phase.

Aromatic acid derivatives with alkyloxy or alkyl terminal groups are known to show mesomorphism due to the dimerization of their carboxylic acid groups through hydrogen bonding. In these cases, the intermolecular hydrogen bonds between hydroxyl groups results mesomorphism. A series of aromatic–aliphatic polyester amide shows thermotropic liquid crystallinity through the lateral H-bonded between interaction amide linkages. The lateral H-bond interaction is also effective for the molecular arrangement of smectic C phase for these mesogen complexes exhibiting stable mesophase.

In continuation of our work on design, synthesis [12–17] and characterization [18–23] of various types of supramolecular hydrogen-bonded liquid crystals (SMHBLCs), in this article, we represent the results of two homologous series of double SMHBLC possessing mesogenic ligand of p-n-alkyloxy benzoic acids and a non-mesogenic moiety of aliphatic carboxylic acids.

2. Experimental

2.1. Materials

The p-n-alkyloxy benzoic acids *n*BAO and dodecane dicarboxlic acid are supplied by Sigma Aldrich, (Germany) and dimethyl formamide (DMF), solvent High Performance Liquid Chromatography (HPLC) grade were purchased and used as received.

2.2. Synthesis of Hydrogen Bonded Liquid Crystal Homologous Series

2.2.1. SA+nBAO and PA+nBAO Homologous Series. Intermolecular double hydrogen-bonded mesogens are synthesized by the addition of two moles of *n*BAOs with one mole of Suberic acid/Pimelic acid in N,N- DMF, respectively. Further, they are subject to constant stirring for 12 hours at ambient temperature 30°C till a white precipitate in a dense solution is formed. The white crystalline crude complexes are obtained by removing excess DMF

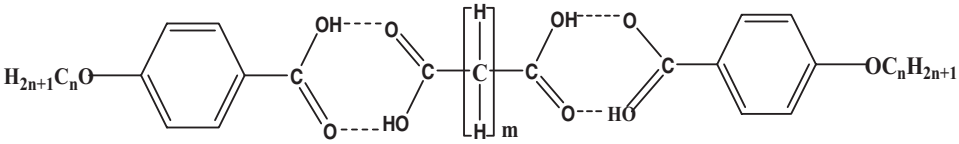

Figure 1. Molecular structure of X+nBAO (where X = SA when $m = 6$ and X = PA when $m = 5$).

and are recrystallized with dimethyl sulfoxide (DMSO). The molecular structures of the present homologous series of p-n-alkoxy benzoic acids with suberic acid/pimelic acid are depicted in the Fig. 1, where n represents the alkyloxy carbon number and m is number of H-C-H spacers groups, here $m = 6,5$.

2.2.2. Instrumentation. Optical textural observations were made by Nikon polarizing microscope which was well equipped with Nikon digital charge-coupled device camera system (Tokyo, Japan) having 5 mega pixels and 2560 × 1920 pixel resolutions. The liquid crystalline textures were processed, analyzed, and stored with the aid of ACT-2U imaging software system (Tokyo, Japan). The temperature control of the LC cell was equipped by Instec, HCS402-STC 200 temperature controller (Colorado, USA) to a temperature resolution of ±0.1°C. This unit was interfaced to a Pentium computer by IEEE–STC 200 to control and monitor the temperature. The LC sample was filled by capillary action in its isotropic state into a polyamide buffed sample cell (Instec, USA) of about 4 micron spacer. The transition temperatures and corresponding enthalpy values were experimentally obtained by Differential Scanning Calorimeter (DSC) by Shimadzu DSC-60 (Tokyo, Japan). The Fourier Transform Infra Red spectroscopy (FTIR) spectra was recorded on KBr pellets by ABB FTIR MB3000 spectrometer (Burlington, Canada) and analyzed with the MB3000 software. The chemical structures of these complexes were analyzed with Nuclear Magnetic Resonance spectrometer, Brucker International ULTRA SHIELD Model (East Milton, Canada). The 300 MHz NMR spectrum of complexes was recorded in $CDCl_3$ with tetramethyl silane as an internal standard.

3. Results and Discussion

The mesogens prepared are insoluble in water and sparingly soluble in common organic solvents such as methanol, ethanol, benzene, and dichloro methane. However, they show a high degree of solubility in coordinating solvents such as DMSO and pyridine. All these mesogens melt at specific temperatures below 126.1°C (Tables 1 and 2). They show high thermal and chemical stability when subjected to repeated thermal scans performed during polarizing optical microscope (POM) and DSC studies.

3.1. Fourier Transform Infrared Spectroscopy

FT-IR spectra of free p-n-alkyloxy benzoic acid, Suberic acid, Pimelic acid, and their intermolecular H-bonded complexes are recorded in the solid state (KBr) at room temperature. Figure 2 illustrates the FTIR spectra of the hydrogen-bonded complex of SA+12BAO in solid state at room temperature (30°C). The solid state spectra of free alkyloxy benzoic acid is reported [24] which confirms two sharp bands at 1685 and 1695 cm^{-1} due to the frequency ν(C=O) mode. The doubling feature of this symmetrical stretching mode confirms the dimeric nature of alkyloxy benzoic acid at room temperature [24].

Table 1. Phase transition temperatures of SA+*n*BAO homologous series obtained by DSC. Enthalpy values in J/g are given in parenthesis

	Phase variance		Crystal melt	N	C	F	Crystal
12	NCF	DSC (h)	94.3 (75.12)	120.1 (37.84)			
		DSC (c)		112.6 (1.98)		81.3 (25.14)	63.7 (28.21)
		POM		113.1	111.5	81.4	63.8
11	NCF	DSC (h)	96.56 (87.11)	111.0 (3.38)	119.8 (19.93)		
		DSC (c)		118.3 (2.41)	113.2 (1.87)	107.0 (14.45)	79.3 (24.11)
		POM		119	113.6	107.2	79.3
10	NCF	DSC (h)	87.2 (25.88)	93.7 (10.90)	102.6 (2.47)	119.7 (33.74)	
		DSC (c)		124.4 (4.3)	110.1 (3.14)	106.2 (5.28)	85.2 (27.73)
		POM		124.9	110.5	106.4	85.3
9	NCF	DSC (h)	93.50 (90.48)	113.7 (1.75)	119.27 (10.00)		
		DSC (c)		118.5 (3.56)	111.8 (1.58)	101.0 (11.82)	83.21 (27.12)
		POM		119.1	112.2	101.3	83.23
8	NCF	DSC (h)	87.2 (56.63)	102.95 (3.05)	120.3 (48.01)		
		DSC (c)		128.87 (1.97)	109.7 (0.92)	101.5 (26.81)	85.5 (27.60)
		POM		117.8	110.0	101.7	85.5
7	NCF	DSC (h)	91.3 (80.20)		118.2 (21.93)		
		DSC (c)		123.9 (1.00)	116.9 (1.41)	104.5 (7.3)	76.0 (51.15)
		POM		124.3	117.3	104.7	76.1
6	NCF	DSC (h)	99 (47.96)	119.4 (26.84)			
		DSC (c)		125.0 (3.77)	113.6 (0.54)	103.9 (22.44)	86.2 (52.96)
		POM		124.4	113.4	103.5	86
		DSC (h)	115.2 (147.77)				
5	NCF	DSC (c)		119.7 (3.65)	111.2 (3.26.)	101.7 (4.95)	99.6 (78.60)
		POM		119.0	111.3	101.8	99.5

Table 2. Phase transition temperatures of PA+*n*BAO homologous series obtained by DSC. Enthalpy values in J/g are given in parenthesis

n	Phase variance		Crystal melt	N	C	F	G	Crystal
12	NCF	DSC (h)	95.6 (104.58)					
		DSC (c)		125.5 (4.26)	94.8 (2.55)	83.1 (2.47)		82 (35.23)
		POM		126	95.2	83.2		82
11	NCF	DSC (h)	97.7 (159.5)	109.2 (0.1)	120.0 (0.5)			
		DSC (c)		121.1 (2.94)	103.2 (1.35)	93.40 (0.39)		81.2 (135.64)
		POM		121.7	103.6	93.6		81
10	NG	DSC (h)	87.2 (30.26)	94.23 (35.78)				
		DSC (c)		98.9 (4.83)			87.0 (16.27)	73.0 (32.64)
		POM		99.6			87.5	73.2
9	NG	DSC (h)	93.52 (110.66)					
		DSC (c)		108.1 (8.89)			91.9 (5.37)	88.4 (77.18)
		POM		109			92.4	88.5
8	NG	DSC (h)	75.52 (57.46)	91.92 (92.83)				
		DSC (c)		105.0 (11.09)			87.7 (29.72)	74.0 (32.40)
		POM		105.6			87.8	74.1
7	NG	DSC (h)	89.16 (137.0)					
		DSC (c)		104.3 (8.19)			74.1 (13.88)	71.6 (37.22)
		POM		104.7			74.2	72.6
6	NG	DSC (h)	91.25 (85.64)					
		DSC (c)		108.3 (6.92			81.6 (33.11)	71.5 (39.12)
		POM		108.6			81.7	71.5
		DSC (h)	95.4 (56.20)	113.5 (41.50)				
5	NG	DSC (c)		109.8 (4.30)			105.9 (40.80)	77.5 (48.40)
		POM		110.3			106.1	77.5

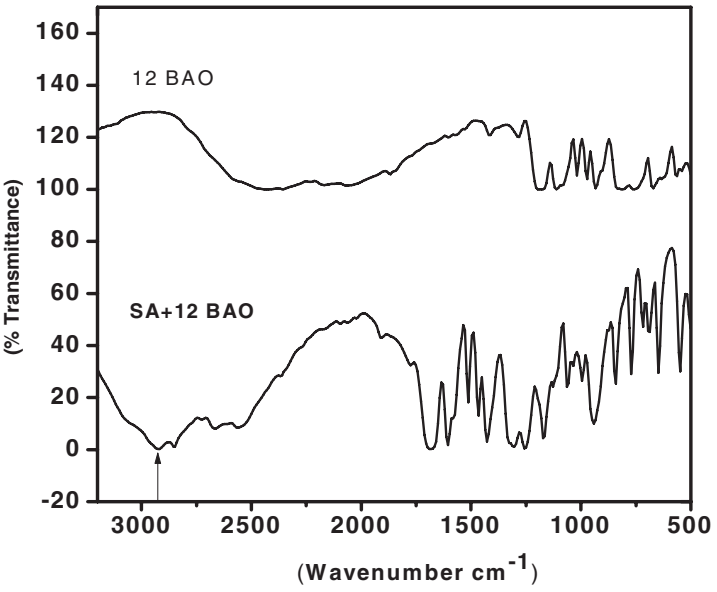

Figure 2. FTIR spectra of SA+12BAO complex.

3.1.1. FTIR studies of SA+12BAO homologous series. The FT-IR spectra of SA+12BAO complex shows absorption band at 1427 cm^{-1} that is attributed to the O-H in plane bending coupled with C-O stretching vibrations, while O-H stretching absorption band appears at 2924 cm^{-1}. The presence of H-bonding in the present complex is further inferred by the appearance of new band of ν (O-H) at 2921 cm^{-1}. The doubling nature of ν(C=O) mode may be attributed to the dimeric nature of the acid group at room temperature [24]. Corresponding spectrum of solution state (chloroform) shows a strong intense band suggesting the existence of monomeric form of benzoic acid. A noteworthy feature in the spectra of SA+12BAO complex is that the appearance of a broad band at 1690 cm^{-1} and nonappearance of the doubling nature of ν(C=O) mode of benzoic acid moiety. This clearly suggests that the dimeric nature of the benzoic acid dissociates and prefers to exist in a monomeric form upon complexation.

Similar results are obtained for all the complexes of PA+*n*BAO homologous series. Thus from FTIR studies the hydrogen bond formation in both the above series have been identified and confirmed.

3.2. ^{1}H-NMR Studies of SA+12BAO and PA+11BAO Homologous Series

The chemical structures for SA+*n*BAO and PA+*n*BAO series have been verified by ^{1}H-NMR studies. As a representative case ^{1}H-NMR for SA+12BAO and PA+11BAO complexes are discussed. The recorded spectra are shown in Figs 3 and 4 and the following chemical shifts were observed:

(1) Broad resonance peaks are observed approximately in the range of 0.5–2.8 ppm for methylene protons. In SA+12BAO complex, these characteristic peaks are observed between 2.292 and 0.856 ppm and in PA+11BAO complex, these signals

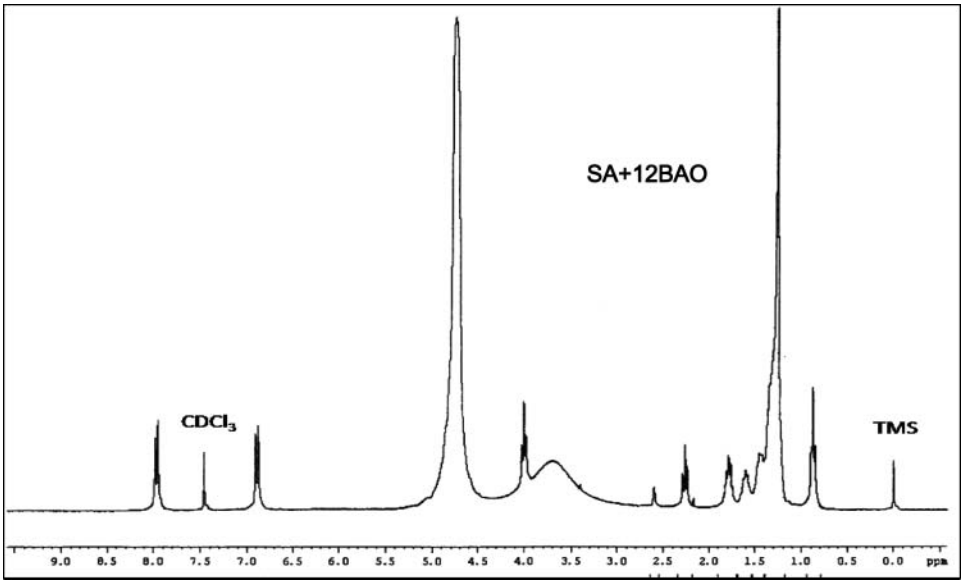

Figure 3. [1]H-NMR spectra of SA+12BAO complex.

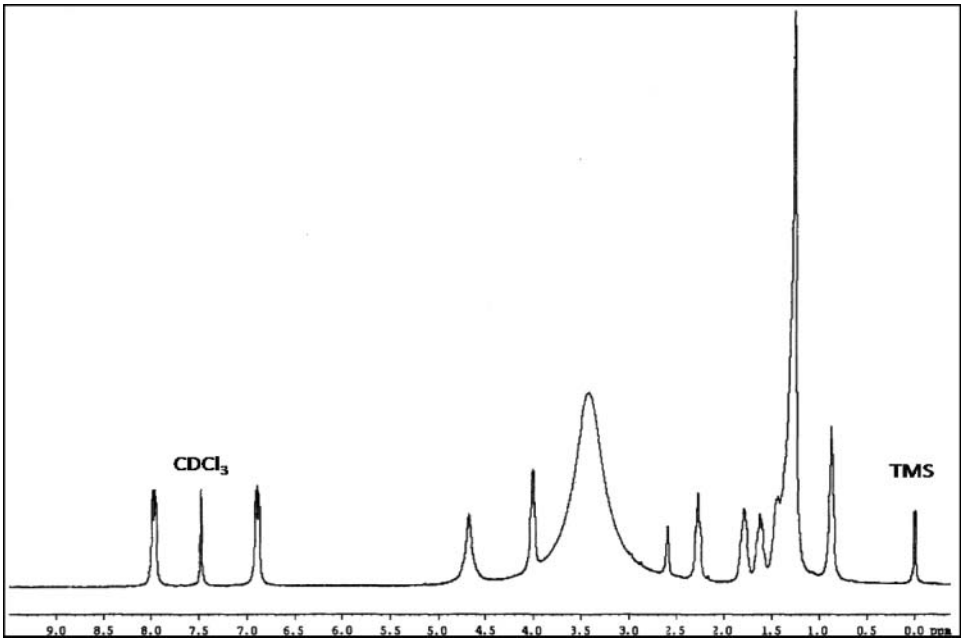

Figure 4. [1]H-NMR spectra of PA+11BAO complex.

are observed between 2.594 and 0.867 ppm which corresponds [25] to the existence of backbone methylene protons.

(2) Two set of multiplets between 6.883–6.913 and 7.957–7.986 ppm in SA+12BAO complex, 6.884–6.907 and 7.954–7.978 ppm in PA+11BAO complex are due to aromatic protons, respectively [25].

(3) Existence of the methoxy proton unit resonance shows a characteristic peaks between 3.985–4.028 ppm in SA+12BAO and 3.997–4.009 ppm in PA+11BAO complex, respectively.

3.3. Textural Studies of SA+nBAO Homologous Series

The mesogens of suberic acid and alkyloxy benzoic acid homologous series were found to exhibit three phases with characteristic textures [26], viz., Nematic (droplets, Plate 1), smectic C (broken focal conic, Plate 2) and smectic F (chequered board texture, Plate 3) respectively. The general phase sequence of the suberic acid and alkyloxy benzoic acids can be shown as:

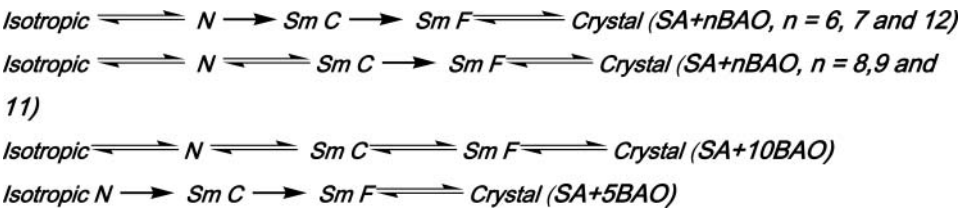

3.3.1. PA+nBAO Homologous Series. The mesogens of the pimelic acid and alkyloxy benzoic acid homologous series are found to exhibit four phases with characteristic textures [26], viz., Nematic (Fine droplets (Plate 4), smectic C (broken focal conic, Plate 5), smectic F (chequered board texture, Plate 6), and smectic G (smooth multicolored mosaic structure, Plate 7) phases, respectively. The general phase sequence of the pimelic acid and alkyloxy benzoic acids can be shown as:

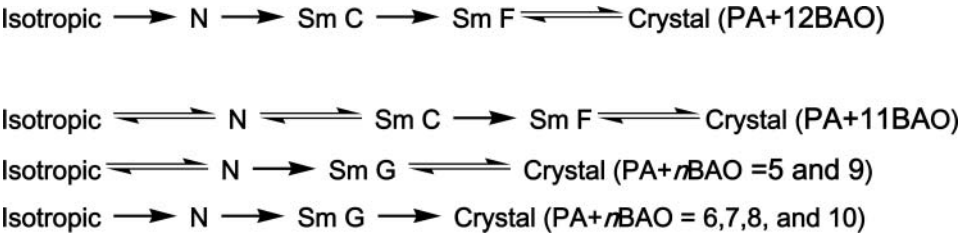

3.4. DSC Studies

DSC thermograms are obtained in heating and cooling cycle. The sample is heated at a scan rate of 10°C/min in N_2 atmosphere and hold at its isotropic temperature for 1 min so as to attain thermal stability. The cooling run is performed with the same scan rate of 10°C/min. The respective equilibrium transition temperatures and corresponding enthalpy values of the mesogens of the homologous series were recorded and tabulated as Table 1. POM studies also confirm these DSC results.

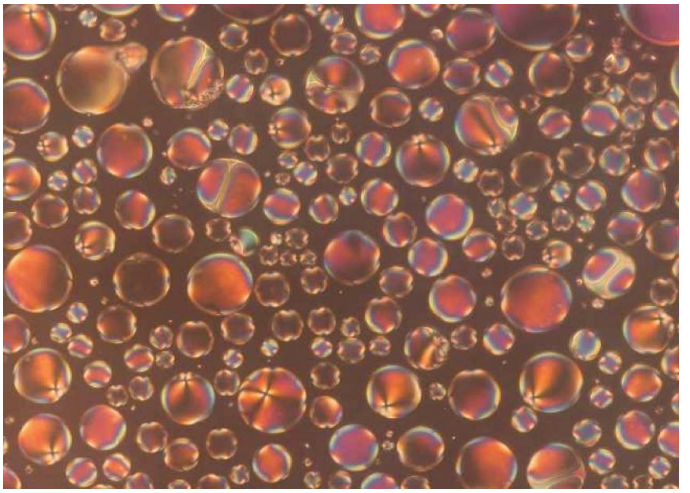

Plate 1. Nematic droplets texture in SA+*n*BAO complex.

3.4.1. DSC Studies of PA+nBAO Homologous Series. As a representative case, the phase transition temperatures and enthalpy values of alkoxy benzoic acid and pimelic acid mesogen (PA+5BAO) is discussed. Figure 5 illustrates the thermogram of PA+5BAO hydrogen-bonded complex recorded at a scan rate of 10°C·min for the heating and cooling run. The cooling run of DSC thermogram shows three distinct transitions namely isotropic to nematic, nematic to smectic G, and smectic G to crystal with transition temperatures 109.8°C, 105.9°C, 77.5°C, and corresponding enthalpy values 4.30, 40.8, and 48.40 J/g, respectively. While in the heating cycle two distinct transitions, namely, crystal to melt, melt to nematic are obtained at 95.4°C, 113.5°C with corresponding enthalpy values of 56.20 and 41.50 J/g, respectively. These transition temperatures of the present homologous series agree with

Plate 2. Broken focal conic texture of smectic C in SA+*n*BAO complex.

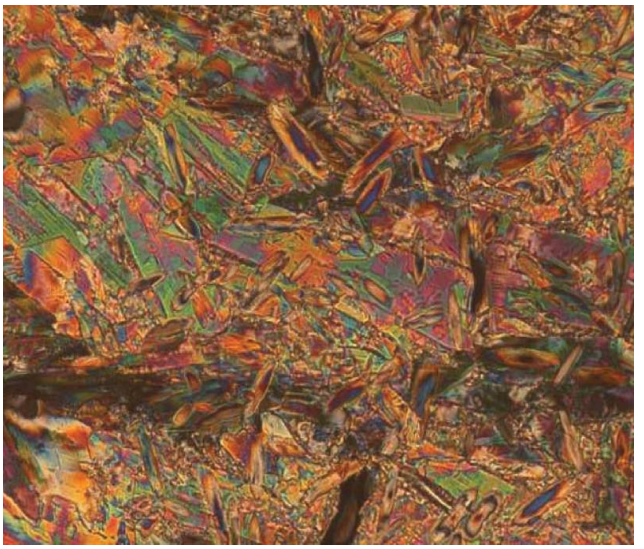

Plate 3. Chequered board texture of smectic F in SA+*n*BAO complex.

optical polarizing microscopic studies. Here, isotropic to nematic and smectic G to crystal is enantiotropic transitions, and nematic to smectic G is monotropic transition.

3.5. Phase Diagram of p-n-alkoxybenzoic Acid

The phase diagram of a p-n-alkoxybenzoic acid is reported earlier [27] which comprises of nematic and smectic C phases.

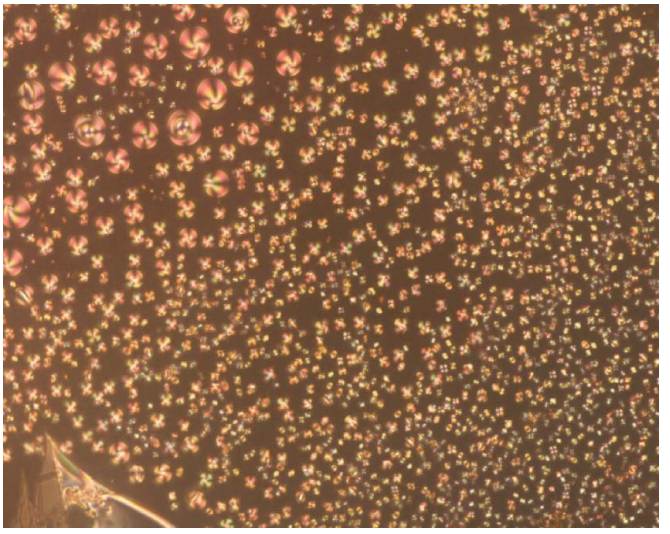

Plate 4. Nematic droplets texture in PA+*n*BAO complex.

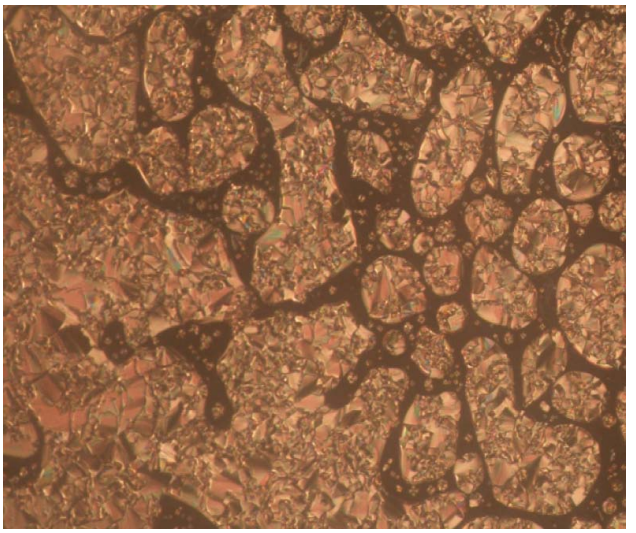

Plate 5. Broken focal conic texture of smectic C in PA+*n*BAO complex.

3.5.1. Phase Diagram of SA+nBAO Homologous Series. The phase diagram of a suberic acid with p-n-alkyloxy benzoic acid complex is depicted in Fig. 6(a). A careful observation of the Fig. 6(a) reveals the following points:

(1) The phase diagram is composed of three phases, namely, nematic, smectic C, and smectic F.
(2) Odd–even effect is present in isotropic to nematic transitions.
(3) In the entire homologous series, all the three phases are present.
(4) Crystallization temperature as well as isotropic temperature mostly decreases with increases in carbon number.

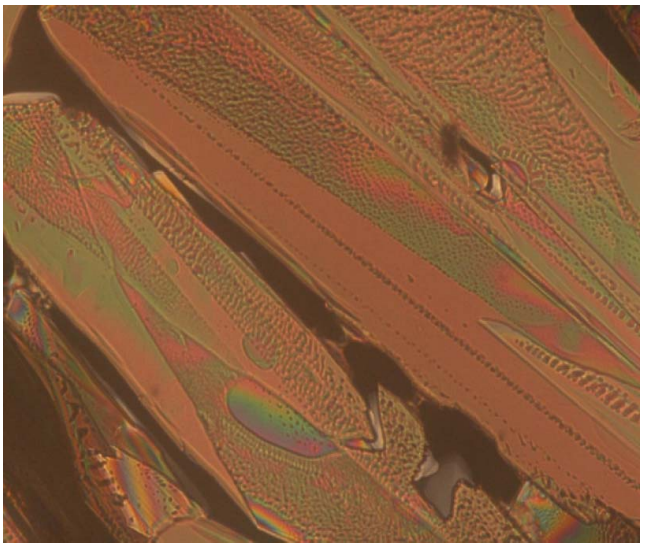

Plate 6. Checkered board texture of smectic F in PA+nBAO complex.

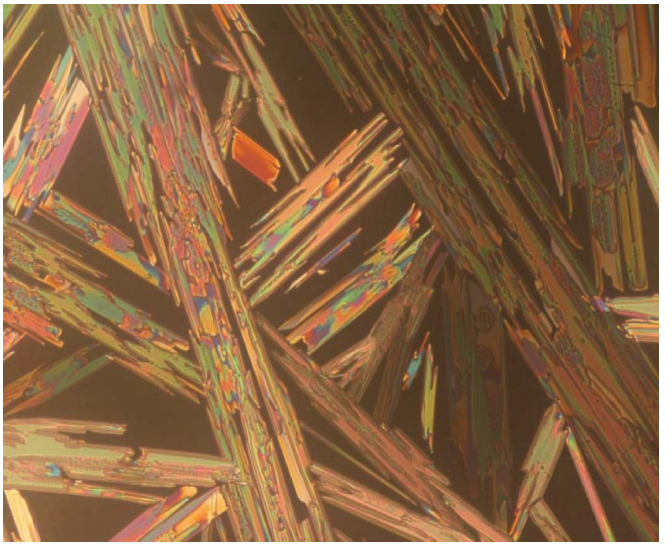

Plate 7. Smooth multicolored mosaic texture of Smectic G in PA+*n*BAO complex.

3.5.2 Phase Diagram of PA+nBAO Homologous Series. The phase diagram of pimelic acid with p-n-alkyloxy benzoic acid complexes is shown in Fig. 6(b). A careful observation of the Fig. 6(b) reveals the following points:

(1) The phase diagram is composed of four phases, namely, nematic, smectic C, smectic F, and smectic G.
(2) Smectic C phase is induced in higher homologues, viz., 11 and 12. This is in accordance with l/d ratio possessed by the series.
(3) Except PA+11BAO and PA+12BAO complexes all the compounds exhibits smectic G phase.

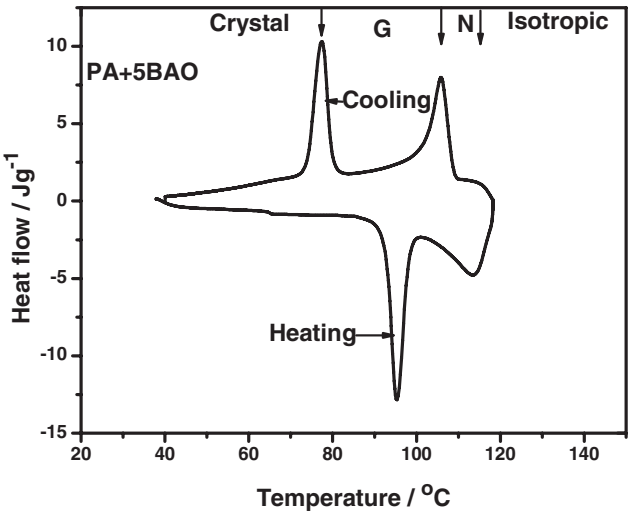

Figure 5. DSC thermogram of PA+5BAO complex.

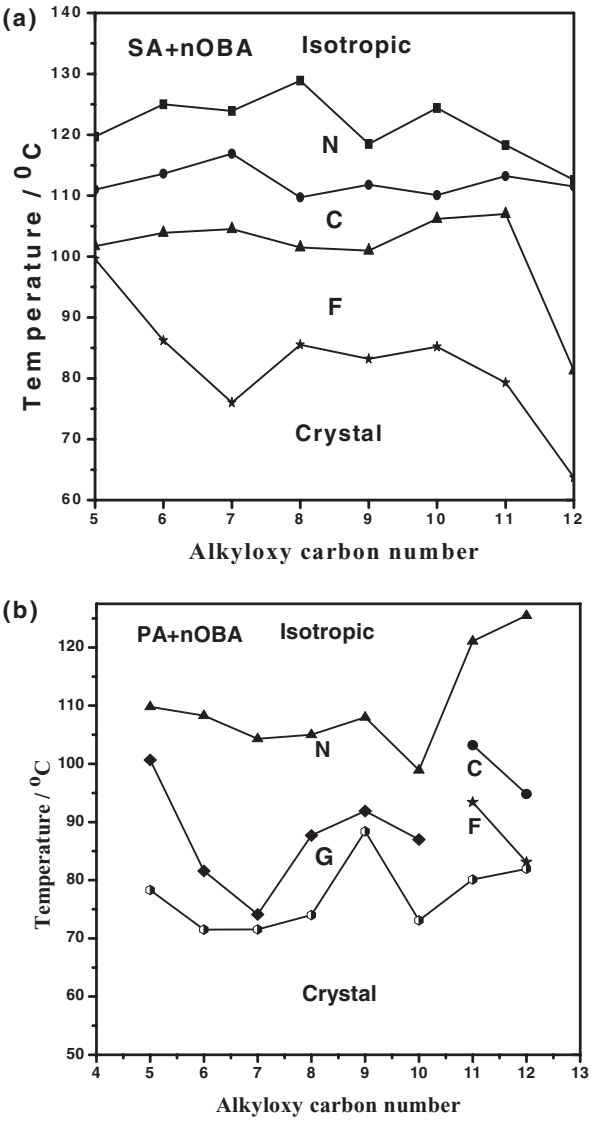

Figure 6. (a) Phase diagram of SA+*n*BAO homologous series. (b) Phase diagram of PA+*n*BAO homologous series.

(4) It is interesting to note that as the chain length increases the phase polymorphism is also enhanced.
(5) Smectic C and F phases are induced in PA+11BAO quenching nematic and smectic G thermal ranges.

4. Odd–Even Effect in SA+*n*BAO Homologous Series

In the present SA+*n*BAO homologous series, odd–even effect is noticed. A plot is constructed with the enthalpy values corresponding to the isotropic to nematic phase transition.

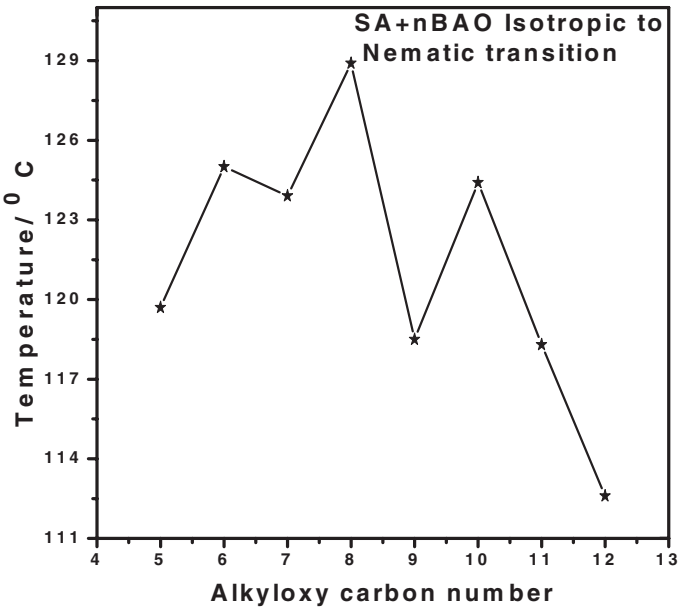

Figure 7. Odd–even effect in SA+*n*BAO homologous series (nematic to smectic C transitions).

From Fig. 7, it can be observed that the magnitudes of the enthalpy values corresponding to the even homologous carbon number exhibit one type of behavior, while the odd counter parts show a different increment. Such behavior has been reported in the literature [28,29] and is referred as odd–even effect. But a small disagreement takes place after SA+11BAO complex. The transition temperature decreases, which in real is to be increased for the SA+12BAO complex.

It may be noted that the present liquid crystalline molecule is composed of rigid and flexible parts as depicted in Fig. 10. The rigid part being the alkyloxy benzoic acid moiety while the flexible moiety is mostly composed of the hydrogen-bonded frame. The rigid core length various with increment in the benzoic acid carbon number. The enriched liquid crystalline phase polymorphism and the associated enthalpy values with increment of alkyloxy carbon number are thus attributed to this part of the chemical structure. Hence, the rigid core plays a vital role in establishing the pronounced odd–even effect as evinced in the present homologous series.

5. Optical Tilt Angle Studies

Optical tilt angle has been experimentally measured by optical extinction method [30] in the smectic C of (SA+*n*BAO, $n = 5$–12 expect 6) and (PA+*n*BAO, $n = 11$ and 12) hydrogen bonded complexes that are depicted in Figs. 8 and 9, respectively. In all the above figures the theoretical fit obtained from the mean field theory is denoted by a solid line. From Figs. 9 and 10, it is observed that the tilt angle increases with decreasing temperature and attains a saturation value. These large magnitudes of the tilt angle are attributed [31] to the direction of the soft covalent hydrogen bond interaction that spreads along molecular long axis with finite inclination. SA+10BAO complex has lower tilt angle value while the SA+7BAO complex exhibits higher magnitude. Tilt angle is a primary order parameter

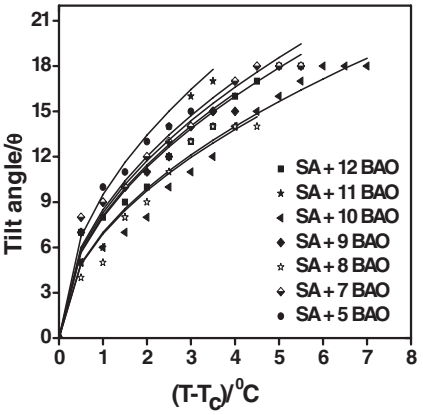

Figure 8. Temperature variation of tilt angle in smectic C phase for SA+nBAO series.

[32] in LC phases, viz., smectic C phase. The temperature variation is estimated by fitting the observed data of $\theta(T)$ to the relation

$$\theta(T)\,\alpha\,(T - T_c)^{\beta}. \tag{1}$$

The critical exponent β value is estimated by fitting the data of $\theta(T)$ to the above Eq. (1) is found to be 0.50 to agree with the Mean Field [32] prediction. The solid line in Figs. 8 and 9 depicts the fitted data. Further, the agreement of β with Mean Field value indicates the long-range interaction of transverse dipole moment for the stabilization of tilted smectic C phases.

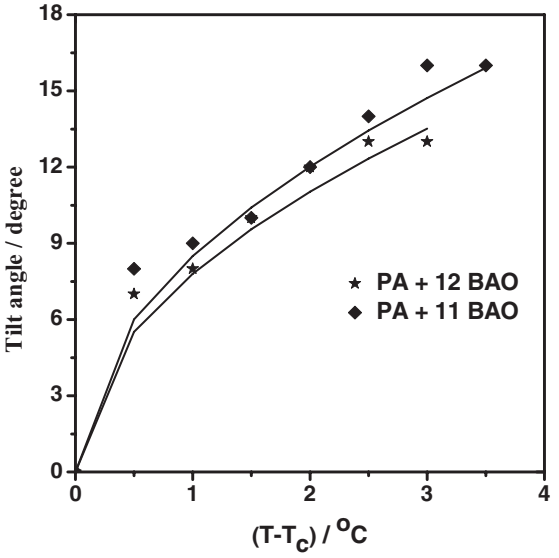

Figure 9. Temperature variation of tilt angle in smectic C phase for PA+nBAO series.

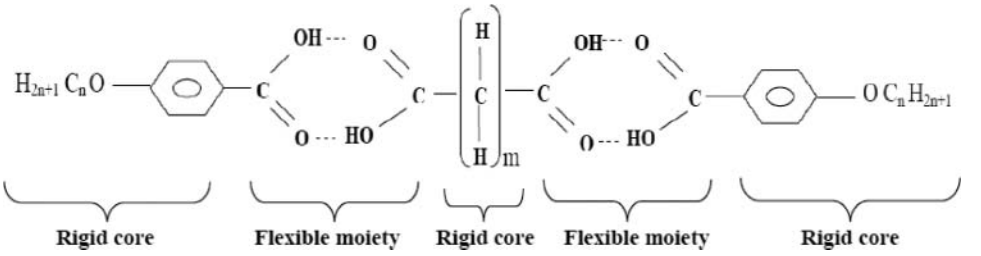

Figure 10. Molecular modeling indicating various types of cores in X+nOBA series.

6. Influence of Spacer Groups on Liquid Crystallinity

Homologous series SA+*n*BAO and PA+*n*BAO have different number of spacer group H-C-H. The number of spacer group H-C-H in SA+*n*BAO series is 6, while it is 5 in PA+*n*BAO. The increment in spacer groups influenced phase variants and liquid crystallinity. Comparing SA+*n*BAO and PA+*n*BAO series, the increment in the spacer group H-C-H has the following effects:

(1) SA+*n*BAO has three phase variants, namely nematic, smectic C, and smectic F, while in PA+*n*BAO (except PA+12BAO and PA+11BAO) complexes, it has two phase variants, namely, nematic and smectic G. Thus the phase variants have been increased with increased number of spacer groups.
(2) Increased spacer group induced two highly ordered phases, namely, smectic C and smectic F in SA+*n*BAO complexes compared to PA+*n*BAO complexes except PA+12BAO and PA+11BAO complexes.
(3) The clearing temperatures (isotropic to nematic) in both the series (SA+*n*BAO and PA+*n*BAO) are almost unaltered. Thus, the increased spacer groups have no influence on the clearing temperatures.
(4) With the increment in the spacer groups, the length of the molecule (l) has increased for the same inter planar distance (d) that in turn influenced the l/d ratio. This altered l/d ratio of SA+*n*BAO complexes favored inducement of the tilted phases.

Acknowledgments

The authors thank infrastructural support provided by Bannari Amman Institute of Technology and gratefully acknowledge the financial support rendered by the Board of Research in Nuclear Sciences (BRNS) of Department of Atomic Energy (DAE), India (Sanction No. 2012/34/35/BRNS).

References

[1] Kato, T., & Frechet, J. M. J. (1989). *J. Am. Chem. Soc.*, *111*, 8533.
[2] Kato, T., Mizoshita, N., & Kishimoto, K. (2006). *Angew. Chem. Int. Ed.*, *45*, 38.
[3] Wang, Y. J., Yan, L. L. M. T., & Yu, J. (2007). *Chin. Chem. Lett.*, *18*, 1009.
[4] Qiu, Y. P., Tang, L. M., Wang, Y., & Guan, S. Y. (2008). *Chin. Chem. Lett.*, *19*, 868.
[5] Yang., L. Y., Shi, M. M., Wang, M., & Chen, H. Z. (2008). *Chin. Chem. Lett.*, *19*, 1260.
[6] Lehn, J. M. et al. (1995). *Supramolecular Chemistry: Concepts and Perspectives*, VCH: Weinheim.

[7] Braga, D., Grepioni, F., & Orpen, A. G. (Eds.), (1999). *Crystal Engineering: From Molecules and Crystals to Materials*, Kluwer Academic Publishers: Dordrecht.
[8] Braga, D., & Grepioni, F. (2000). *Acc. Chem. Res.*, *33*, 601.
[9] Lehn, J. M. (1996). *Supramolecular Chemistry*, VCH: Weinheim.
[10] Muthukumar, M., & Ober, C. K. (1997). Thomas EL. Competing interactions and levels of ordering in self-organizing polymeric materials. *Science*, *277*, 1225.
[11] Kihara, H., Kato, T., Uryu, T., & Fréchet, J. M. (1996). Supramolecular liquid crystalline networks built by self-assembly of multifunctional hydrogen-bonding molecules. *J. Chem. Mater.*, *8*, 961–968.
[12] Vijayakumar, V. N., Murugadass, K., & Madhu Mohan, M. L. N. (2009). *Mol. Cryst. Liq. Cryst.*, *515*, 39.
[13] Vijayakumar, V. N., Murugadass, K., & Madhu Mohan, M. L. N. (2009). *Braz. J. Phys.*, *39*, 601.
[14] Vijayakumar, V. N., & Madhu Mohan, M. L. N. (2009). *Ferroelectrics*, *392*, 81.
[15] Vijayakumar, V. N., & Madhu Mohan, M. L. N. (2010). *Sol. State Sci.*, *12*, 142–149.
[16] Vijayakumar, V. N., & Madhu Mohan, M. L. N. (2009). *Solid State Commun.*, *149*, 2090–2097.
[17] Vijayakumar, V. N., & Madhu Mohan, M. L. N. (2009). *Braz. J. Phys.*, *39*, 600.
[18] Vijayakumar, V. N., Murugadass, K., & Madhu Mohan, M. L. N. (2010). *Mol. Cryst. Liq. Cryst.*, *517*, 41.
[19] Vijayakumar, V. N., & Madhu Mohan, M. L. N. (2010). *Mol. Cryst Liq.Cryst.*, *517*, 111.
[20] Vijayakumar, V. N., & Madhu Mohan, M. L. N. (2010). *Mol. Cryst. Liq. Cryst.*, *524*, 54.
[21] Vijayakumar, V. N., and Madhu Mohan, M. L. N. (2009). *J. Optoelectron. Adv. Mater.*, *11*(8), 1139.
[22] Chitravel, T, Vijayakumar, V. N., & Madhu Mohan, M. L. N. (2010). *Mol. Cryst. Liq. Cryst.*, *524*, 131.
[23] Subhapriya, P., Vijayakumar, V. N., Vijayanand, P. S., & Madhu Mohan, M. L. N. (2011). *Mol. Cryst. Liq. Cryst.*, *537*, 36–50.
[24] Nakamoto, K. (2009). *In Infrared and Raman Spectra of Inorganic and Co-ordination Compounds*, Interscience: New Jersey.
[25] Pavia, D. L., Lampman, G. M., and Kriz, G. S. (2007). *Introduction to Spectroscopy*, Thomson Learning Inc.: India.
[26] Gray, G. W., & Goodby, J. W. G. (1984). *Smectic Liquid Crystals: Textures and Structures*, Leonard Hill: London.
[27] Vijayakumar, V. N., Murugadass, K., & Madhu Mohan, M. L. N. (2009). *Mol. Cryst. Liq. Cryst.*, *515*, 39.
[28] Chandrasekhar, S. (1977). *Liquid Crystals*, Cambridge University Press: New York.
[29] Patel, J. S., & Goodby, J. W. (1987). *Mol. Cryst. Liq. Cryst.*, *144*, 117.
[30] Barmatov, E. B., Bobrovsky, A., Barmatova, M. V., & Shibaev, V. P. (1999). *Liq. Cryst.*, *26*, 581.
[31] De Gennes, P. G. (1974). *The Physics of Liquid Crystals*, Oxford Press: London.
[32] Stanley, H. E. (1971). *Introduction to phase Transition and Critical Phenomena*, Clarendon Press: London.